Applied Thermal Engineering 264 (2025) 125433

Contents lists available at ScienceDirect

Applied Thermal Engineering

journal homepage: www.elsevier.com/locate/apthermeng

Research Paper

Parametric optimisation of diesel–methanol injection timings of a dual-fuel marine engine operating with high methanol fraction using CFD

Panagiotis Karvounis *, Gerasimos Theotokatos

Maritime Safety Research Centre, Department of Naval Architecture, Ocean, and Marine Engineering, University of Strathclyde, Glasgow G4 0LZ United Kingdom

ARTICLE INFO

Keywords:
Decarbonisation
Methanol
Marine engine
Direct injection
Optimisation

ABSTRACT

Although methanol is a transition fuel to decarbonise the shipping industry, its wider use is hindered by several challenges including the dual fuel combustion of high methanol fractions in marine engines. This study aims to parametrically optimise the injection settings for a large marine four-stroke dual-fuel engine of 10.5 MW nominal power considering three representative loads of the operating envelope. The closed cycle of one engine cylinder is modelled in CONVERGE. The CFD model for the diesel mode is first developed and subsequently extended for the dual fuel (methanol–diesel) mode considering 90 % methanol energy fraction. The model is validated against experimental data for the engine diesel and dual fuel operation. Parametric runs with different methanol and pilot diesel injection timings are conducted to identify the settings that achieve the objectives of increased thermal efficiency and reduced NOx emissions considering the constraints pertaining to stable combustion conditions. Results indicate that injecting methanol during the compression stroke (80 ^{o}CA BTDC) and diesel at (12 ^{o}CA BTDC) achieves combustion efficiency up to 99 % and indicated thermal efficiencies of 46 %, 45 %, and 43 % for high, medium, and low loads, respectively, whilst compiling with IMO Tier III limits for NOx emissions. The novelty of the study lies in the setup of a widely applicable CFD model for methanol fuelled marine engines; compliance with IMO Tier III limits and identification of the optimal injection timings ensuring combustion stability, reducing NOx emissions, and improving thermal efficiency. The study provides insights for the development of methanol fuelled marine dual fuel engines.

1. Introduction

Shipping emissions including greenhouse gases and pollutants contribute to climate change and air pollution, impacting both human health and environment [1]. Key contributors to emissions reduction in the maritime industry is the wide adoption of low and zero carbon fuels [2]. Methanol has emerged as a promising option due to its potential to reduce greenhouse gas (GHG) emissions and meet stringent emissions regulations [3]. Its lower carbon content and cleaner combustion characteristics make it an attractive alternative to conventional fossil fuels [4]. Methanol, a versatile alcohol-based fuel, has gained attention as a potential alternative fuel for marine engines. Several studies focused on combustion characteristics of methanol fuel in compression ignition engines compared to diesel operation [5,40–42].

Recent studies dealt with the optimisation of various engine characteristics such as piston bowl, injector(s) position, orientation, and injection settings. Li et al. [6] numerically investigated the performance of a dual-fuel engine with direct injection of both methanol and pilot diesel fuel, considering the following parameters: methanol nozzle diameter, methanol injection pressure, as well as the deflection and divergence angles of the diesel and methanol injectors. The study found that reducing the methanol nozzle diameter from 0.4 mm to 0.3 mm increased the in-cylinder pressure and peak heat release rate due to faster methanol evaporation, while the ignition delay and combustion duration remained unaffected. In contrast, changes to the methanol injection pressure and the diesel and methanol injector angles had only a slight impact on the engine's performance.

Several studies investigated the effects of methanol injection timing and other parameters on engine performance and emissions in dual-fuel engines. Park et al. [7] found that using a 15 % methanol energy fraction (MEF) blend and advancing the methanol injection timing to 0–8 °CA before top dead centre (BTDC) resulted in a 3 % decrease in brake thermal efficiency (BTE) and a 20 % increase in NOx emissions, attributed to higher in-cylinder temperatures. However, the advanced injection timing also improved BTE by shortening the combustion duration. Saxena and Maurya [9] reported that retarding the methanol injection timing increased the maximum pressure rise rate, which could be

* Corresponding author.
E-mail address: panagiotis.karvounis@strath.ac.uk (P. Karvounis).

https://doi.org/10.1016/j.applthermaleng.2025.125433
Received 6 November 2024; Received in revised form 27 December 2024; Accepted 3 January 2025
Available online 4 January 2025

Nomenclature

B_0	Model constant for droplet breakup (−)
C_0	Model constant for droplet breakup (−)
$C_{i,\varepsilon}$	Empirical constant in the ε-equation (−)
CA50	Crank Angle where 50% of the combustion is completed (°)
CA90	Crank Angle where 90% of the combustion is completed (°)
D	Mass diffusion coefficient (m^2/s)
D_d	Droplet diameter (m)
E	Total energy per unit mass (J/kg)
G_k	Turbulence production term (m^2/s^3)
g	Gravitational acceleration vector (m/s^2)
k_k	Turbulent kinetic energy (m^2/s^2)
k_t	Thermal conductivity (W/mK)
LHV	Lower Heating Value (kJ/kg)
m_i	Mass flow rate (kg/s)
n	Number of collected data for RMSE (−)
p	Cylinder pressure (Pa)
R_i	Source term for species reaction (kg/m^3s)
RMSE	Root Mean Square Error
S	Source term in the energy equation (W/m^3)
SOI	Start Of Injection (°CA)
T	Temperature (K)
t	Time (s)
u	Velocity (m/s)
Y_i	Mass fraction of species *i* (−)
y_i	Measured parameter
$\widehat{y_i}$	Calculated parameter
UM	Unburned Methanol (g/kWh)

Greek Variables

ε (m^2/s^3)	Dissipation rate of turbulent energy
θ (°)	Crank angle degree
μ (Pa s)	Dynamic viscosity
μ_t (Pa s)	Turbulent viscosity
ρ (kg/m^3)	Density
σ (N/m)	Surface tension
τ (Pa)	Stress tensor

Abbreviations

ATDC	After Top Dead Centre
BTDC	Before Top Dead Centre
BTE	Brake Thermal Efficiency
CA	Crank Angle
CFD	Computational Fluid Dynamics
DF	Dual Fuel
DI	Direct Injection
EGR	Exhaust Gas Recirculation
IMO	International Maritime Organisation
IVC	Inlet Valve Closing
LHS	Lati Hypercube Sampling
LHV	Lower Heating Value
MEF	Methanol Energy Fractions
NOx	Nitrous Oxides
PISO	Pressure Implicit Splitting of Operators solver
TDC	Top Dead Centre

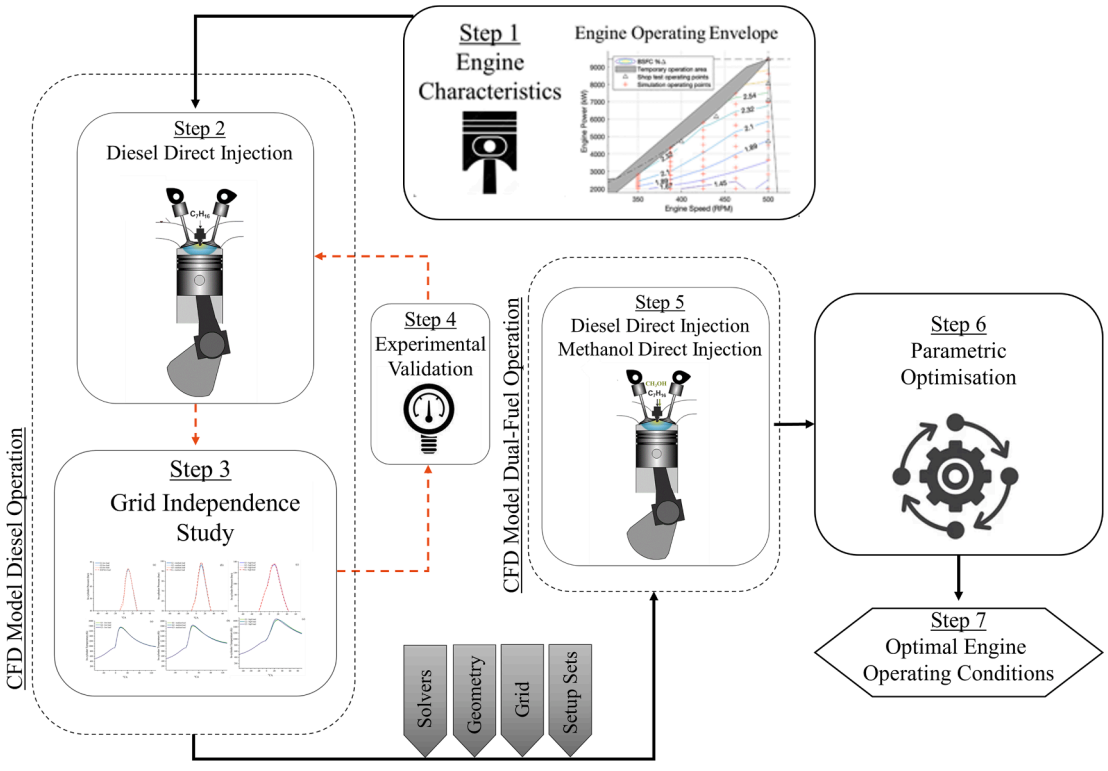

Fig. 1. Methodology flowchart.

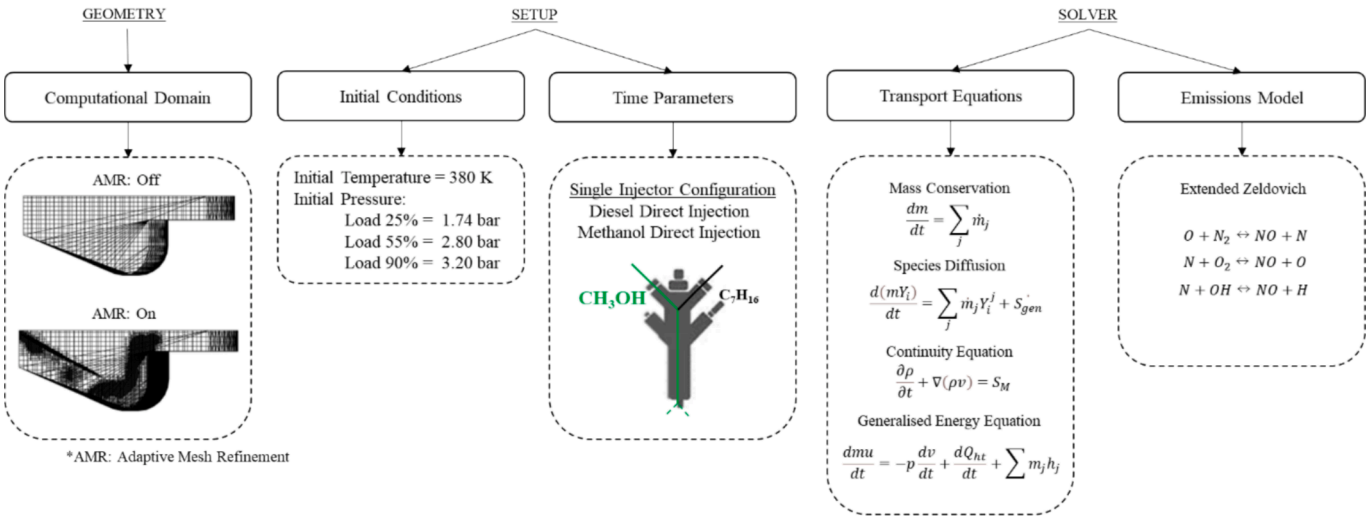

Fig. 2. Developed CFD model characteristics including sub-models, geometry, initial conditions, time parameters and governing equations.

Table 1
Computational grid characteristics.

Parameter		Grid 1	Grid 2	Grid 3	Grid 4
Final element size (mm)		12	10	8	6
Maximum Number of Cells*		10900	18838	36800	87216
Adaptive mesh refinement		On	On	On	On
Velocity Max Embedding Level		3	3	4	4
Temperature Max Embedding Level		3	3	4	4
p_{max} error (%)	low load	0.3	0.3	0.2	0.2
	medium load	0.5	0.2	0.1	0.3
	high load	0.7	0.5	0.3	0.5
p_{cyl} RMSE (bar)	low load	1.48	1.49	1.52	1.53
	medium load	0.97	0.83	0.79	0.78
	high load	1.23	1.40	1.52	1.53
Solution duration (h)		2	3	8	22

* At TDC not including embedding and mesh refining.

Table 2
Investigated marine engine characteristics.

Parameter	Value
Type	Wärtsilä 9L46C
Max Power Output (kW)	10500
Maximum Speed (rpm)	500
Number of Cylinders (–)	9
Compression Ratio (–)	14.0:1
Bore / Stroke (mm)	460 / 580
Diesel Start of Injection (°CA)	variating (10–120 °CA BTDC)
Diesel Injection Pressure (bar)	1000
Nozzle Angle (deg)	67.5
Spray Cone Angle (deg)	17.5
Nozzle Diameter (mm)	0.78
Number of holes (–)	6
Simulation Cycle Period; IVC–EVO	135 °CA BTDC–135 °CA ATDC

mitigated by employing a double injection strategy. They also found that methanol accumulation near the cylinder walls led to unburned fuel and increased emissions. Rodriguez-Fernandez et al. [10] studied a heavy-duty diesel engine using a 35 % MEF, evaluating the effects of intake pressure and temperature, EGR rate, injection angle, diesel injection pressure, and pilot fuel ratio, concluding that low-temperature and highly premixed combustion conditions along with exhaust gas recirculation (EGR) can lead to improved efficiency and lower emissions.

Wang et al. [8] studied the optimisation of injection timing and intake manifold temperature for 17 % MEF, concluding that an injection timing of 7.4°CA BTDC and an intake temperature of 388 K improved BTE by 7 % at high loads. Sener et al. [11] studied the optimisation of the combustion chamber geometry, spray angle, and injection pressure, whereas Enoki et al. [12] investigated the optimisation of diesel and methanol injection timings, identifying the optimal methanol injection timing in the range of 2–3 °CA before diesel injection and highlighting the impact of the pre-combustion chamber geometry on fuel mixing. Ning et al. [13] experimentally studied the effects of methanol injection timing and methanol fraction on the performance and emissions of a single-cylinder direct-injection engine, reporting the trade-offs between these parameters. Li et al. [14] conducted a multi-objective optimisation study on a methanol-diesel dual-fuel direct injection engine, considering the methods of reactivity-controlled compression ignition and direct dual-fuel stratification. To improve the engine performance and reduce emissions, the following recommendations were provided: increase the injection pressure to promote the spray penetration, air–fuel mixing, and efficient combustion; increase the EGR rate to minimise NOx emissions and knock intensity; use an early diesel start of injection; and employ small diesel and medium methanol spray angles.

Li et al. [15] optimised the injector position, orientation, and start of injection of both methanol and diesel fuels for 65 % MEF. They concluded that the higher charging temperature and early injection of pilot fuel is deemed essential to enhance in-cylinder reactivity and therefore methanol combustion efficiency. Shi et al [16] examined a 70 % MEF at low loads of a methanol/diesel engine with both fuels directly injected in-cylinder. The study revealed that two-stage injection strategy allows for complete combustion of methanol fuel. Diesel is injected at early stage of the compression process at 25 °CA BTDC. However, the in-cylinder temperature increases favouring NOx emissions formation. Soni et al. [17] showcased that EGR is essential for methanol combustion and simultaneous NOx emissions reduction. The study considered 15 % MEF and NO emissions reduced by 27 % compared to the diesel mode. Karvounis et al. [18] numerically studied up to 90 % MEF in marine engines with in-cylinder direct injection resulting in higher indicated thermal efficiency and significant NOx emissions reduction.

The preceding literature review reveals the lacks optimisation studies for marine engines operating with high methanol energy fractions (MEFs). To address this gap, this study aims at parametrically optimising the injection timings for the methanol and pilot diesel of a marine four-stroke medium-speed engine operating with high methanol fraction considering three representative loads (low, medium and high) whilst evaluating the engine compliance with international NOx Tier III limits. CFD modelling of a single engine cylinder is employed to estimate the engine performance and emissions parameters. The parametric optimisation considers the objectives of indicated thermal efficiency and

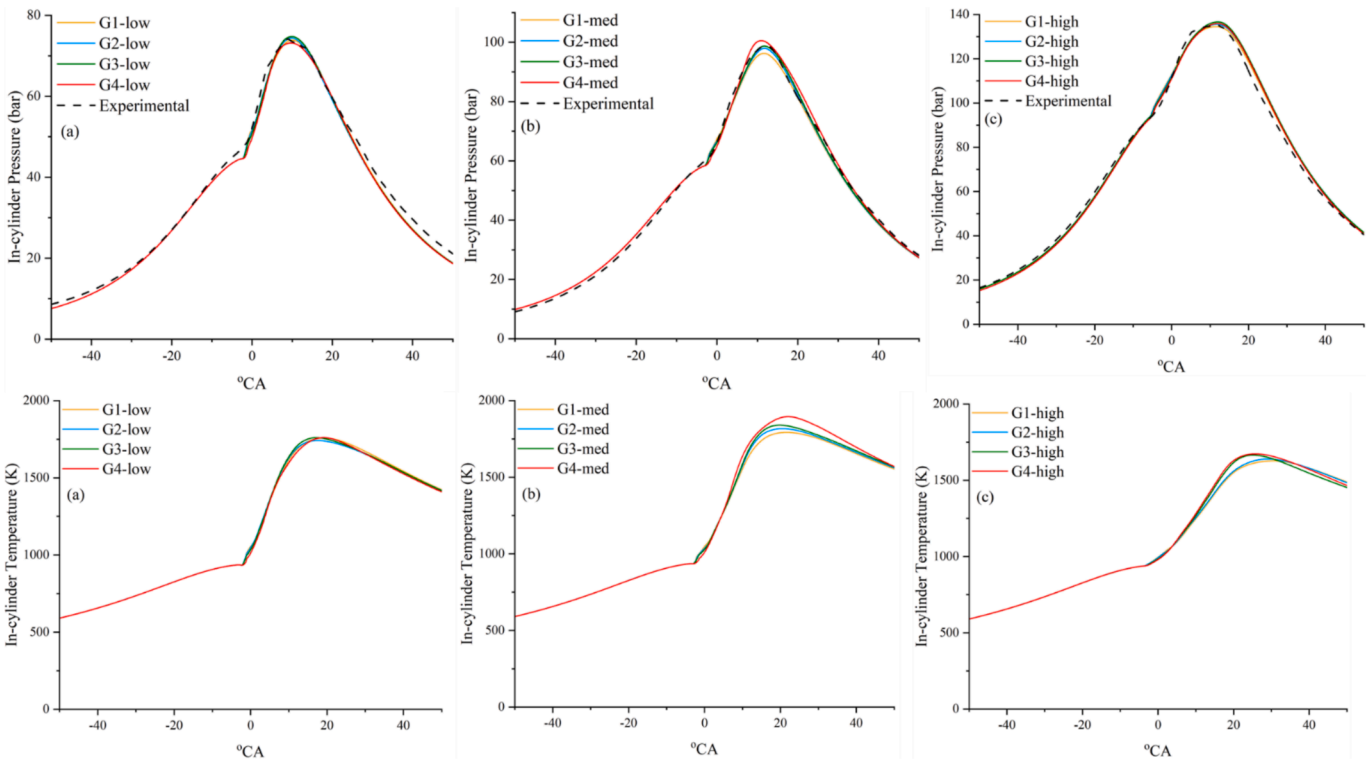

Fig. 3. Grid sensitivity study results on in-cylinder pressure and temperature for: (a) low load; (b) medium load and; (c) high load.

NOx emissions, as well as constraints on the combustion efficiency (and the respective unburnt methanol emissions).

The novelty of the study stems from the identification of the optimised operating conditions for dual-fuel marine engines utilising a high methanol energy fraction of 90 %, addressing a significant shift towards cleaner fuel compositions. Furthermore, the research seeks to contribute to the advancement of effective strategies for reducing NOx emissions, and improving thermal efficiency, thereby promoting environmental sustainability within the maritime industry. Complementary, the findings demonstrate compliance with IMO Tier III NOx emission standards, showcasing the engine's potential for regulatory alignment. Additionally, the study identifies critical regions prone to misfiring and knocking, enhancing understanding of combustion stability in high-methanol dual-fuel applications. This study provides insights into the optimal operating conditions for marine engines using high methanol fractions.

2. Methodology

The research methodology consists of eight steps, as presented in the flowchart of Fig. 1. Step-1 deals with the collection of engine geometrical characteristics and settings from the manufacturer guides. Furthermore, the engine operating envelope along with the actual operating profiles are reviewed to identify three representative operating points. In specific, 25%, 55% and 90% loads, henceforth denoted as low, medium and high loads respectively, are used in Steps 2–7. Step-2 focuses on the CFD model development in the CONVERGE software. The required boundary and initial conditions are retrieved from the engine zero-dimensional model developed by Tsitsilonis et al. [19]. Step-3 deals with the computational grid sensitivity study to select the grid compromising between computational effort and results accuracy. Step-4 focuses on the CFD models validation against experimental measurements for the engine diesel mode and data reported in the literature for the methanol–diesel (dual-fuel) mode. Step-5 develops the CFD moles for the investigated methanol cases from the validated CFD model (baseline) considering the same solver, geometry, grid particulars, and setup settings. Step-6 focuses on the bi-objective parametric optimisation of the engine injection settings, in specific the start of injection variation of both main (methanol) and pilot (diesel) fuels. The optimisation objectives include the indicated thermal efficiency and NOx emissions. Step-7 determines the optimal engine operating conditions and injection settings.

2.1. CFD model

The developed CFD model characteristics are illustrated in Fig. 2. The computational domain includes a cylinder sector geometry that reduces the required computational effort compared to the full cylinder geometry. The computational grid employs adaptive mesh refinement close to the injector region during the injection phase. The boundary and initial conditions are determined from the previous authors' studies [18,31] and ensure adequate combustion conditions for the 90 % methanol energy fraction (MEF). Tables 4 and 5 (Appendix) provide further details about the computational models and initial conditions, respectively.

The methanol energy fraction (MEF) is defined by the following equation:

$$MEF = \frac{m_{CH_3OH} LHV_{CH_3OH}}{(m_D LHV_D) + (m_{CH_3OH} LHV_{CH_3OH})} \quad (1)$$

where m denotes to the respective fuel mass, and LHV denotes each fuel lower heating value in kJ/kg.

The EGR ratio is calculated according to the following equation:

$$EGR = \frac{m_{EG}}{m_{EG} + m_{air}} \quad (2)$$

The single injector layout is modelled accommodating both methanol and diesel (n-heptane) fuels in-cylinder injection at different timings. The Pressure Implicit Splitting of Operators (PISO) solver is selected for the numerical solution of the density-based Navier-Stokes equations. The extended Zeldovich mechanism is employed to estimate the NOx emissions [21], as it effectively represents the NOx formation during

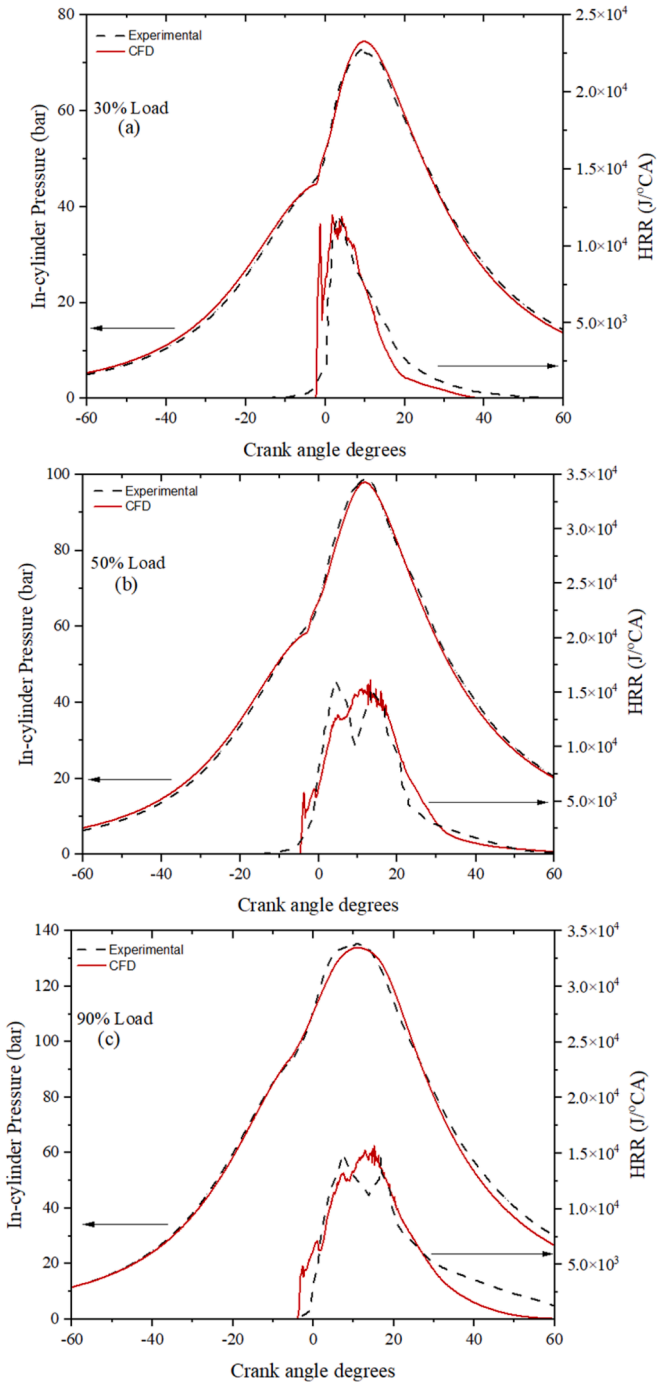

Fig. 4. Experimental validation of in-cylinder pressure and heat release rate for different loads.

Table 3
Baseline operating conditions at the three loads.

Parameter	Low Load	Medium Load	Maximum Load
Compression Ratio	14	14	14
EGR	0	8	12
T_{IVC} (K)	380	380	380
P_{IVC} (bar)	1.74	2.8	3.2

high-temperature combustion considering reactions between N and O_2. It highlights the temperature-dependent production of NOx. Thermal NOx is formed by the oxidation of atmospheric nitrogen present in the combustion air whereas, prompt NOx is produced by high-speed reactions at the flame front. NOx emissions consistency across different loads was ensured by employing a validated CFD model, against experimental data for diesel, natural gas and methanol operation.

The CFD model assumptions are presented in detail in the previous author's study [18].

2.2. Grid Independency study & experimental validation

The CFD model employs an embedded mesh control strategy with and adaptive mesh refinement. The grid dependence study is conducted to determine of the trade-off between computational effort and error whereas the considered grids include elements of 12, 10, 8 and 6 mm. The grids characteristics and performance metrics (percentage error and root mean square error for the in-cylinder pressure) are listed in Table 1.

The marine four-stroke engine with nine cylinders and nominal power of 10.5 MW is studied in different operating conditions. The engine particulars are presented in Table 2 whereas the engine layout is presented in [23]. Shipboard measurements of the in-cylinder pressure and other performance parameters were acquired from this engine during operations of a ferry, as reported in Tsitsilonis et al. [31]. Three operating points, in specific, 30 %, 50 % and 90 % loads, for which measurements were taken, are employed herein as representative of the low, medium and high loads engine operation, as they correspond to the most frequent ship operations.

The root mean square error of the in-cylinder pressure (in the closed cycle), which is used as a metric to assess the CFD model results accuracy, is calculated according to the following equation:

$$RMSE = \sqrt{\left(\frac{\sum_{i=1}^{n}(y_i - \hat{y}_i)^2}{n}\right)} \quad (4)$$

where n denotes the data points number, whereas y_i and $\hat{y}_i$ denote the measured and calculated values of the in-cylinder pressure, respectively.

Fig. 3 provides the derived CFD results for the in-cylinder pressure and temperature for the four grids (G1 to G4) in the three loads (low, medium, and high). For the low, medium and high loads, the in-cylinder maximum pressure percentage errors were found in the ranges of 0.2–0.5 %, 0.1–0.3 %, and 0.3–0.7 % for Grids 1–4. According to the presented results (Table 1 and Fig. 3), Grids 3 and 4 exhibit similar performance. As both grids provide convergence, Grid 3 is selected due to its lower computational effort.

Fig. 4 shows the predicted and measured in-cylinder pressure and heat release rate for the three loads in the diesel mode. The noise from the experimental measurements is reduced by applying filtering. The CFD results exhibit satisfactory matching with the experimental ones, whereas the total brake power output and maximum pressure errors were below 3 %. In both cases, the first law of thermodynamics is employed to calculate the HRR however, the assumptions and input for the heat transfer rate calculation exhibit slight differences.

In the absence of experimental data for marine engines operating with methanol, the CFD model is tested with a more complex combustion process including two fuels (natural gas and pilot diesel) for a marine engine (of similar size with the investigated engine). To that extend, the model is also validated against dual-fuel measurements for the gas operation of the marine engine under pilot diesel injection.

To validate the methanol–diesel combustion model, reported experimental data were used from a small-scale high speed engine operating in the dual-fuel mode with 30 % MEF and premixed conditions in 75 % load [39] (Appendix B). Detailed results of the experimental validation are presented in the previous authors' study [18]. The CFD model exhibits RMSE below 8 % for all the examined modes. Considering these results, the developed CFD model is deemed validated as it exhibits adequate accuracy for both diesel and methanol-diesel modes.

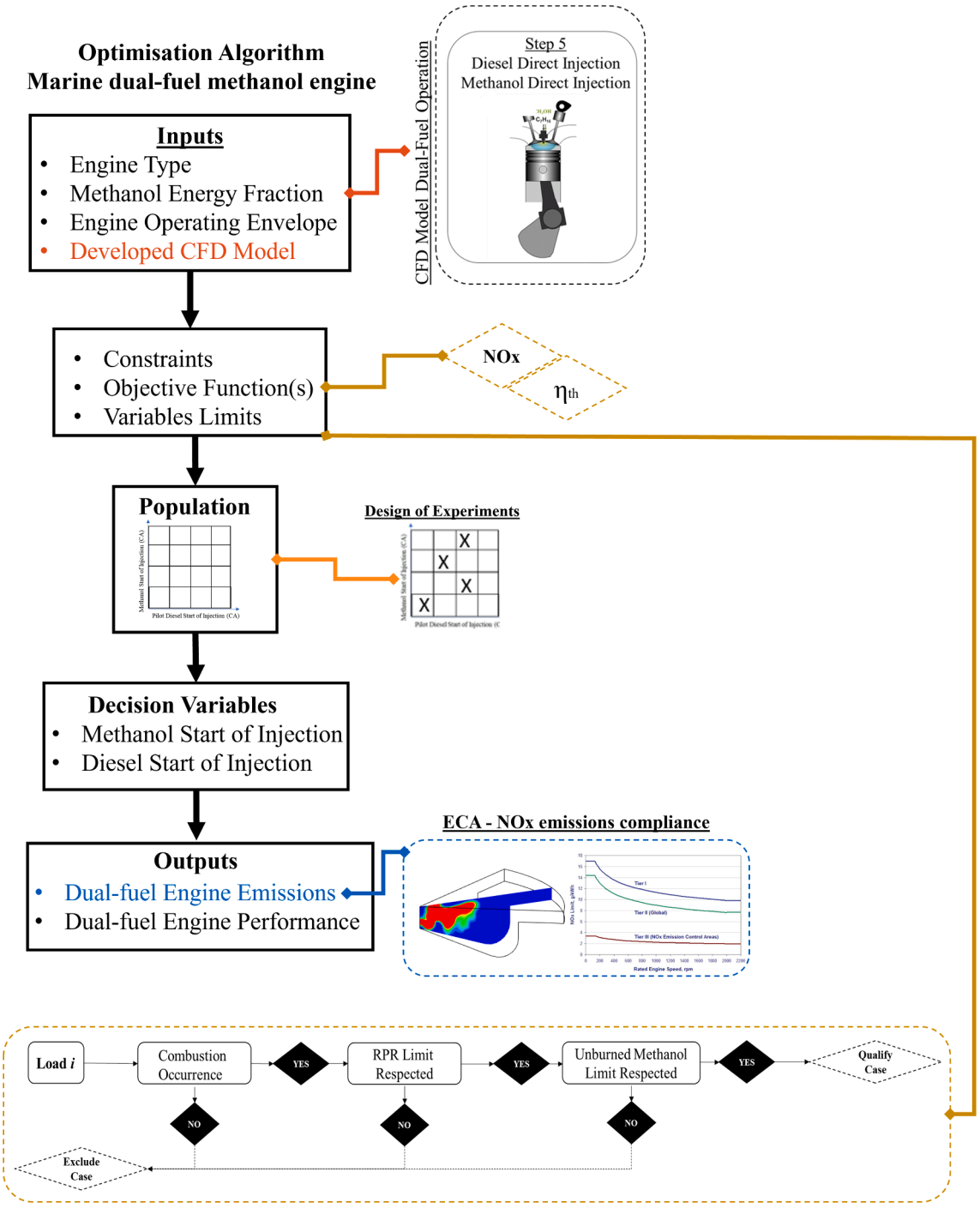

Fig. 5. Parametric optimisation algorithm for enhanced performance and emissions.

2.3. *Parametric optimisation and cases Description*

When the engine is operating at high methanol energy fractions, it is essential to provide optimised operating parameters. It is evident from literature that in-cylinder temperature is an important parameter that determines the combustion characteristics and overall efficiency of the methanol engine [13,24]. Methanol-fuelled engines are prone to combustion instabilities [25]. Due to the high latent heat of vaporisation and low cetane number, methanol fuel, presents significant ignition resistance under low load operation. To that extend, low load operating conditions present a constraint for the other loads of the engine. The investigated engine baseline settings are listed in Table 3, whereas their derivation is discussed in Karvounis et al. [18].

The design of simulations is based on Latin Hyperqube statistical method [26] that generates a sample of plausible values from a multi-dimensional distribution allowing to reduce the number of calculations conducted. The parameters of interest in this study include the injection timings of both main (methanol) and pilot (diesel) fuels. Methanol start of injection variates (SOIM) between 110 °CA BTDC to 10 °CA BTDC with a five-degree timestep. The start of injection of pilot diesel fuel (SOI_D) variates between 4 °CA BTDC and 12 °CA BTDC, while for all the cases the injection pressure is kept constant at 1450 bar. Since EGR is beneficial for NO_x emissions, a mild use of it at 8 % and 12 % is considered for medium and high loads respectively [27] that remains

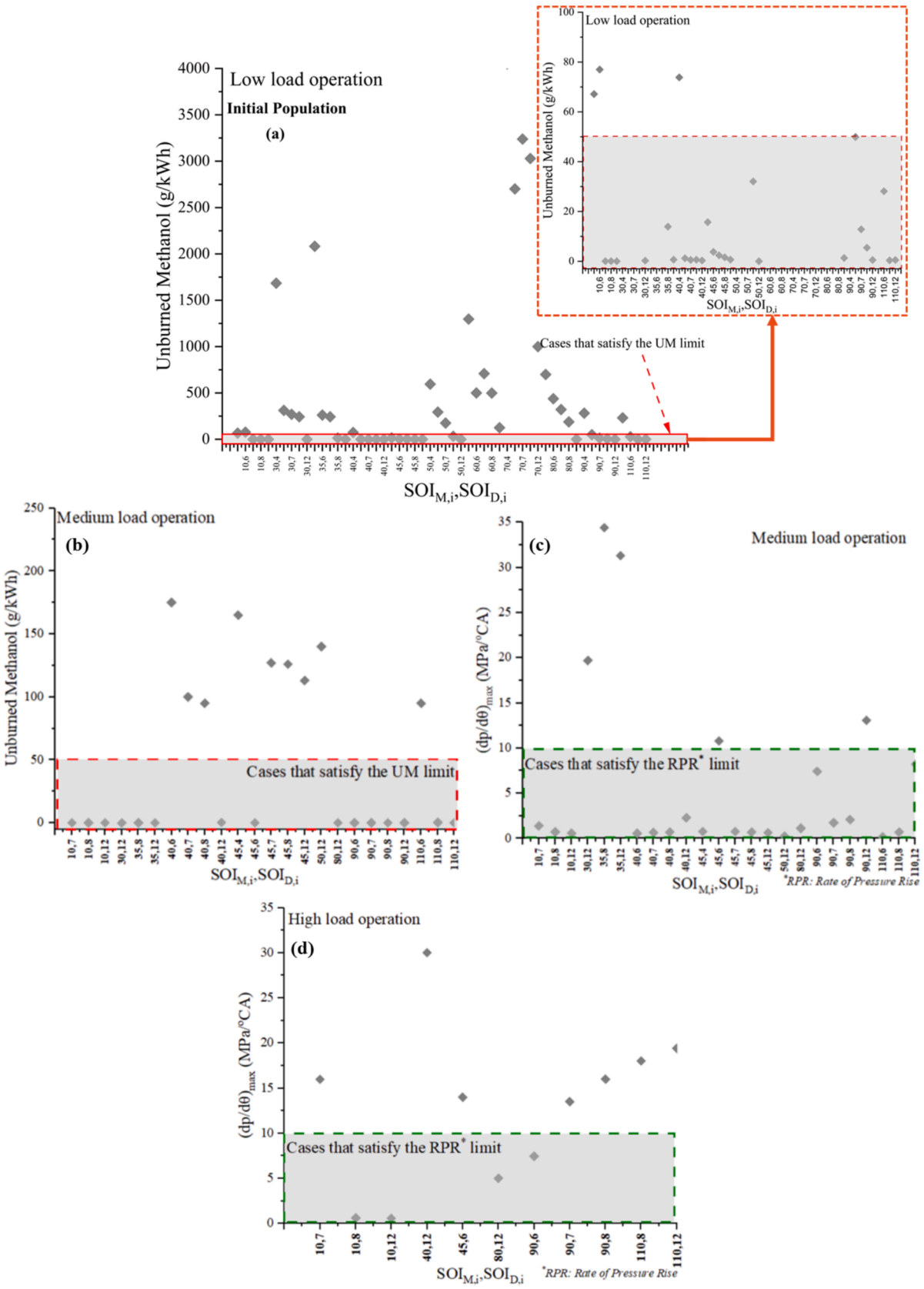

Fig. 6. (a) Initial population of simulated injection timings for low-load operation satisfying the unburned methanol limit. Initial population of cases that are qualified based on low-load operation and satisfy the (b) knocking propensity and (c) unburned methanol limit at medium load and (d) knocking propensity limit at high load.

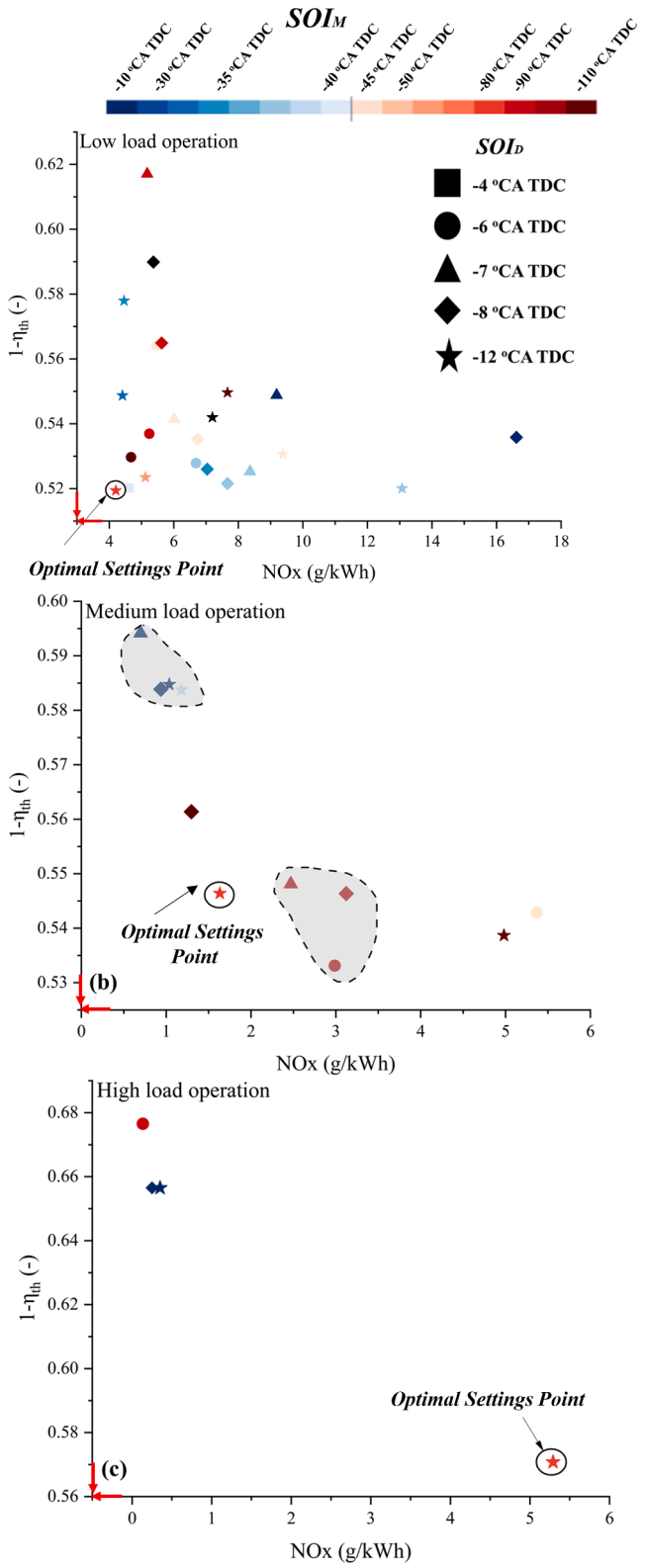

Fig. 7. Bi-objective optimisation of methanol and diesel start of injection for low-load operation.

constant for all cases and variations of which are not examined in this study.

The parametric optimisation objectives include the NOx emissions minimisation and maximum the indicated thermal efficiency maximisation. The following constraints are considered: (a) the unburned methanol (UM) should be lower than 50 g/kWh, which is a value denoting almost complete combustion conditions, and; (b) the rate of maximum in-cylinder pressure rise should be lower than 10 MPa/°CA; which ensures the engine structural integrity. [28]. Constraint (a) is used for the low load (where incomplete combustion is more likely to occur), whereas both constraints are used for the medium and high loads. For low-load operation the UM constraint is followed whereas both constraints are analysed for medium and high-load operation and presented in Eq. (5). The objectives include the minimal NOx emissions and maximum thermal efficiency. The flowchart of the optimisation algorithm is presented at Fig. 5. Other design characteristics, such as the spray angle, injectors diameter and position are not discussed in the present study.

After selecting the optimal injection timings for both fuels, the investigated engine compliance with the IMO NOx Tier limits is assessed according to Eq. (5).

$$\sum_{i=1}^{4} w_i \, BSNOx_i \; < \; BSNOx_{Tier_j} \tag{5}$$

Where i of 1 to 4 correspond to 25, 50, 75 and 100% loads respectively; w_i denotes the weight for each load (being 0.2, 0.5, 0.15 and 0.15 for 25, 50, 75 and 100% loads, respectively); denotes the brake specific NOx emissions for each load; whereas j is II or III, corresponding to Tier II or Tier III, respectively. NOx emissions in different loads for the investigated marine engine are calculated based on the E3 cycle, as reported in ISO 8178 [29].

3. Results

This section discusses the results obtained from the preceding methodology. It includes the selection of the optimal injection timings for both fuels and the emission and performance of the dual-fuel engine. Finaly, compliance with international regulatory standards is examined.

3.1. Injection timings

Fig. 6 shows the CFD model results for the simulated cases with combinations of the methanol and diesel start of injection. For the low load, Fig. 6(a) illustrates the results for the simulate 57 cases, whereas the red lined rectangle includes the cases that satisfy the set unburned methanol limit. As the engine low load operation is associated with low in-cylinder reactivity, several cases correspond to misfiring, whereas several others lead to considerable unburnt methanol. For the medium load , 27 cases satisfy the set unburnt methanol and maximum rate of pressure rise (RPR) limits.The methanol ignition resistance results in misfiring for several cases that with diesel start of injection closer to TDC. Methanol injection closer to TDC (between 30 to 35 °CA BTDC) resulted in high RPR values, which denote potential unstable combustion and knocking.. For the high load operation (Fig. 6d) 4 cases satisfy the set rate of pressure rise limit. The increased in-cylinder reactivity provides the required energy to ignite methanol, hence misfiring does not occur. However, the methanol high laminar flame speed resulted in increased RPR. Methanol injection prior to 80 °CA BTDC results in more homogeneous methanol–air mixture, which in turn causes significant RPR regardless of the diesel start of injection. This leads to only four cases satisfying the RPR limit. The methanol injection range can be extended by using EGR or other knock mitigation techniques.

Fig. 7 presents the CFD results (optimisation objectives of the NOx emissions and indicated thermal efficiency) for the cases satisfying the UM and RPR constraints for the low, medium and high loads. The cases presented satisfy the unburned methanol and RPR limitations. For low load operation (Fig. 7a), most of the cases concentrate around the 43 % to 48 % indicated thermal efficiency (1-η_{th} = 0.52 to 0.57). However, not clear trade-offs are observed between cases. Retarded diesel SOI (6 to 8 °CA BTDC) and methanol SOI (10 to 35 °CA BTDC), benefits the

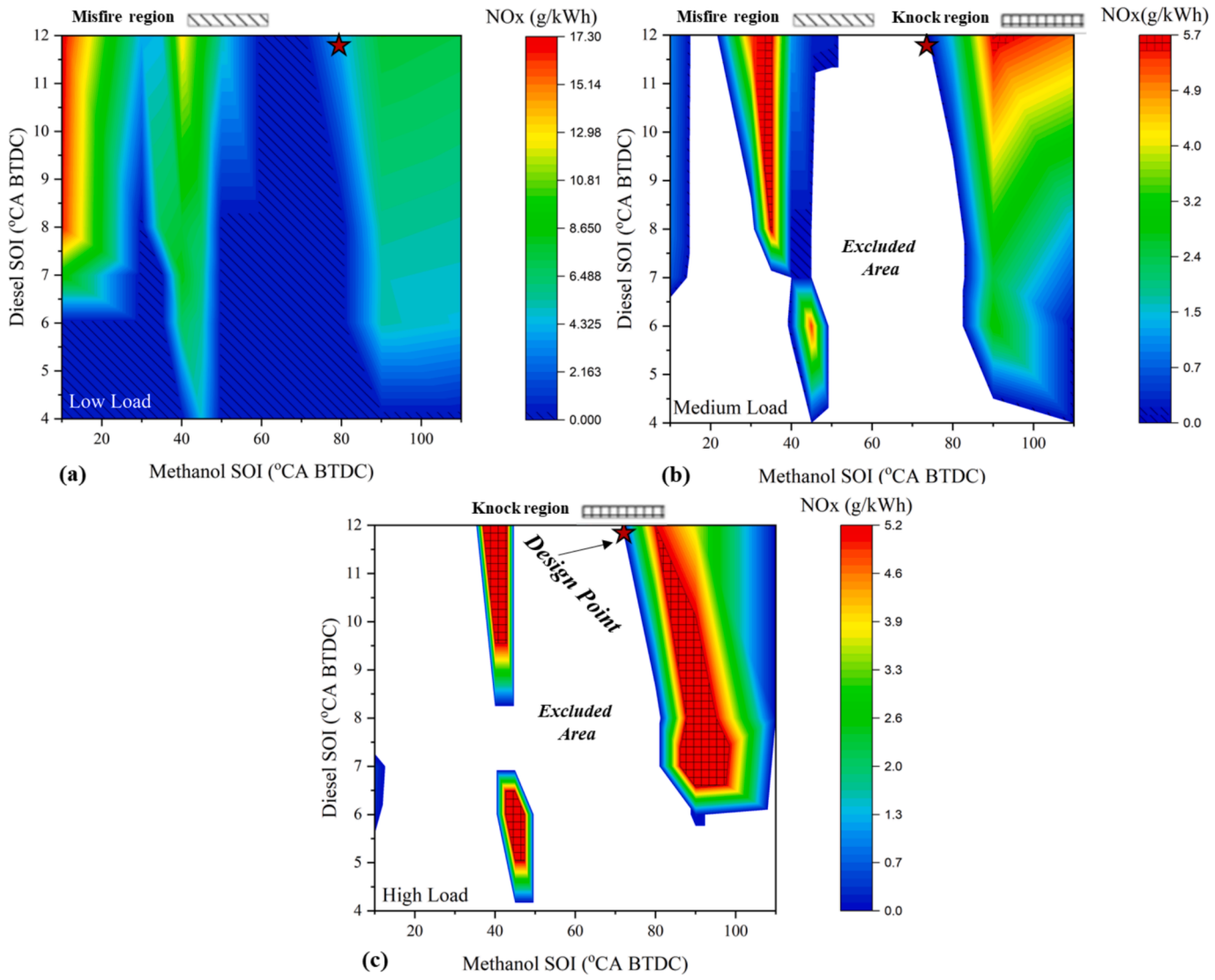

Fig. 8. NOx emissions for the different injection timings of diesel and methanol for (a) low, (b) medium and (c) high load operation.

Table 4
Simulation models characteristics.

Mechanism	Diesel Mode	Dual Fuel Methanol DI
Reaction Mechanism	Andrae and Head [32]	
Combustion	SAGE: Two adaptive zones; Solving analytical Jacobian matrix; Absolute tolerance: 10^{-14}	
NOx Mechanism	Extended Zeldovich [21]: Thermal NOx model; Mass scaling factor to convert NO to NOx: 1.533	
Turbulence Model	RANS k-ε: Provides lower accuracy than LES however extensively used in combustion modelling due to acceptable results at relatively low computational time [33]	
Droplet breakup	KH-RT: Model size constant 0.61, Model velocity constant 0.188 [34]	
	Mass diffusivity constants	
	C7H16D_0 = 5.94 × $10^{-6}n_0$ = 1.6	C7H16 D_0 = 5.94 × $10^{-6}n_0$ = 1.6CH3OHD_0 = 7.9 × $10^{-6}n_0$ = 1.87
Droplets collision model	NTC [35]	
Wall heat transfer	Han & Reitz [36]	
Spray/Wall interaction model	Han [37]	

Table 5
Boundary and initial conditions for the diesel operation model.

Boundary Conditions	Value	Explanation
Cylinder head Temperature (K)	530	Values calculated from 0D thermodynamic model developed by Tsitsilonis et al. [19], corresponding to warmed up conditions.
Cylinder Wall Temperature (K)	430	
Piston Temperature (K)	550	
Initial Conditions		
Temperature at the IVC (K)	380	Calculated assuming ideal gas law and considering the boost temperature and pressure from the shop trials.
Turbulent kinetic energy (m^2/s^2)	62.02	Default values were used. A parametric investigation was conducted to determine these parameters impact on the results.
Turbulent dissipation (m^2/s^3)	17183	
Liquid diesel spray Temperature at the time of injection (K)	340	Within the range of experimental results reported by Payri et al. [38].

efficiency due to faster methanol combustion, which increases the in-cylinder pressure and temperature, hence generating higher NOx emissions.The optimal injection timings at low load is 12 °CA BTDC for diesel SOI and 80 °CA BTDC for methanol. Advancing diesel and

Table 6
Proposed operating conditions for the dual-fuel methanol marine engine.

Load (%)	Methanol Energy Fraction (%)	Pilot Diesel Energy Fraction (%)	Methanol SOI (°CA BTDC)	Pilot SOI (°CA BTDC)	Methanol Injection Duration (°CA)	Pilot fuel Injection Duration (°CA)	CR (–)	T_{IVC} (K)	p_{IVC} (bar)
20	90	10	80	12	22	2	14	380	1.74
55					45	4			2.8
90					67	5			3.2

methanol SOI results in better mixing of methanol and air providing the required energy to combust the methanol-air mixture. Concurrently, the cooling effect of methanol takes place reducing the maximum temperature reached yielding lower NOx emissions. Benefits in the indicated thermal efficiency are also noted since a more homogenous air-methanol mixture is expected to combust quicker. The optimal settings point results at NOx emissions of 4.2 g/kWh and indicated thermal efficiency of 48 %. Further advancing methanol SOI, favours the cooling effect of methanol resulting in greater unburned quantities penalising the efficiency.

For medium load operation (Fig. 7b), clustering of the qualified cases based on the methanol SOI is achievable. The cases with advanced methanol injection result in higher efficiency (45 % to 46.8 %) due to better homogeneity of air-methanol mixture. Retarded methanol injection penalises the efficiency due to unburned methanol induced by incomplete combustion. The identified optimal settings are at 12 °CA BTDC for diesel SOI and 80 °CA BTDC for methanol SOI. This point is selected as the best trade-off between the indicated thermal efficiency (45.3%) and NOx emissions (1.63 g/kWh). For the high load (Fig. 7c) only four comply with unburned methanol and RPR constraints. The retarded methanol injection results in low indicated thermal efficiency (around 34%) due to lowcombustion efficiency. Therefore, the optimal settings of 12 °CA BTDC for diesel SOI and 80 °CA BTDC for methanol SOI are selected, yielding 5.29 g/kWh NOx emissions and 43 % indicated thermal efficiency.

Fig. 8 illustrates the NOx emissions as function of the methanol SOI (horizontal axis) and pilot diesel SOI (vertical axis) for all the investigated cases. Fig. 8a presents the NOx emissions for the low-load operation of the engine variating both pilot and main fuel injection timings. Low load operation is characterised by low in-cylinder reactivity that results to ignition resistance. Close to complete combustion are achieved by advancing the pilot injection (before 8 °CA BTDC) whilst retarding methanol injection close to TDC. This is due to the high-pressure environment close to TDC. However, this leads to increased in-cylinder temperature and hence increased NOx emissions. Methanol SOI between 50 and 75 °CA BTDC results in misfiring, as injected methanol evaporation quenches the diesel flame, leading to incomplete combustion. Methanol SOI before 80 °CA BTDC provides sufficient to form a more homogenous methanol–air mixture. Therefore, higher combustion efficiency is achieved with reduced NOx emissions compared to the methanol injection close to TDC.

At medium-load (Fig. 8c) the reactivity increases in-cylinder and potential knocking phenomena occur depending on the homogeneity of methanol-air mixture. When diesel is injected well before TDC (8 to 12 °CA BTDC) and methanol is injected between 35 and 40 °CA BTDC, complete combustion is achieved, however the rate of pressure rise in-cylinder indicates knocking propensity. The latter can be observed from NOx concentration that is significantly increased due to high temperature in-cylinder. Between 45 and 50 °CA BTDC methanol injection, the heterogeneity of the mixture in-cylinder results in misfire as the methanol quenching effect is still active as demonstrated by Huang et al. [30]. Methanol SOI of 110 °CA BTDC and diesel SOI of 12 °CA BTDC provided NOx emissions of 4.98 g/kWh. This is attributed to the prolongation of the mixing periods for both methanol and diesel, resulting in earlier combustion start, and longer residence time of combustion products at temperature above the cut-off.

For the high-load operation (Fig. 8c) the high oxygen content of methanol fuel, and laminar burning velocity (0.455 m/s at $\Phi = 1$,P = 1 atm, T = 293 K), result in increased knocking tendency under high reactivity cylinder conditions [22,25]. Knock-free operation is achieved for methanol injection between 80 °CA BTDC and 90 °CA BTDC and all examined diesel injection timings. Table 6 summarises the identified optimal SOI settings as well as other parameters including injection durations, temperature and pressure at the inlet valve closing, which are used in the CFD simulations presented in the next sections.

3.2. Dual-Fuel engine characteristics

Fig. 9 shows the in-cylinder pressure and heat release rate for the three different loads which were derived by the CFD model by using the identified optimal injection timings (Table 6). For the low load, the peak pressure is 10.3 MPa whereas the heat release profile is characterised by a premixed phase where a part of methanol that is mixed with air is combusted along with diesel [20]. This is also observed in the respective spatial distribution (Fig. 11) that indicates that combustion occurs arround the jet region. The second peak which corresponds to the maximum value of the heat release rate (9.05 kJ/°CA). Since methanol injection has finished before the start of combustion, partial mixing with air has been achieved and hence premixed flame front is developed in-cylinder. This is demonstrated by the in-cylinder contour provided in Fig. 9a and supported by the pertinent study of Liang et al. [44]. The combustion is almost complete at 12.7 °CA ATDC, where the methanol mass is consumed. For the medium load, the CA50 is delayed to 5.2 °CA ATDC, whereas the combustion duration reduces (CA90 is found at 10.7 °CA ATDC), due to higher in-cylinder reactivity (causing considerably faster methanol combustion). The combustion starts at 10 °CA BTDC, with its premixed part being smaller compared to the low load, which is also evident from the respective in-cylinder temperature spatial distribution (Fig. 11). The peak in-pressure is 17.1 MPa and the peak HRR is 36.6 kJ/°CA. At high loads, the ignition is further retarded to 5 °CA BTDC and combustion duration further reduces (CA90 is found at 4.7 °CA ATDC). The heat release profile is characterised by diffusive flame front whereas fewer mass of methanol is well mixed with air prior to combustion. The maximum pressure achieved is 23.9 MPa and peak HRR is 152.2 kJ. Such high maximum pressure is expected to drive the engine beyond its physical limit. To address that future research is expected to focus on alternative injection strategies, and EGR techniques that would reduce the maximum pressure reached in-cylinder. The detailed performance output of the engine under the optimal injection timings is presented in Table 7.

3.3. Emissions and spatial distribution

Fig. 10 shows the NOx emissions versus the engine load along with the compliance of the investigated engine with the IMO limits. NOx emissions are calculated for four different operating points (25, 50, 75 and 100% loads), whereas the engine NOx emissions (to check compliance) are calculated according to Eq. 5. The NOx emissions was found 2.5 g/kWh and is well below the Tier II limit (10.9 g/kWh) and marginally lower than the Tier III limit (2.68 g/kWh). For the 25% load,

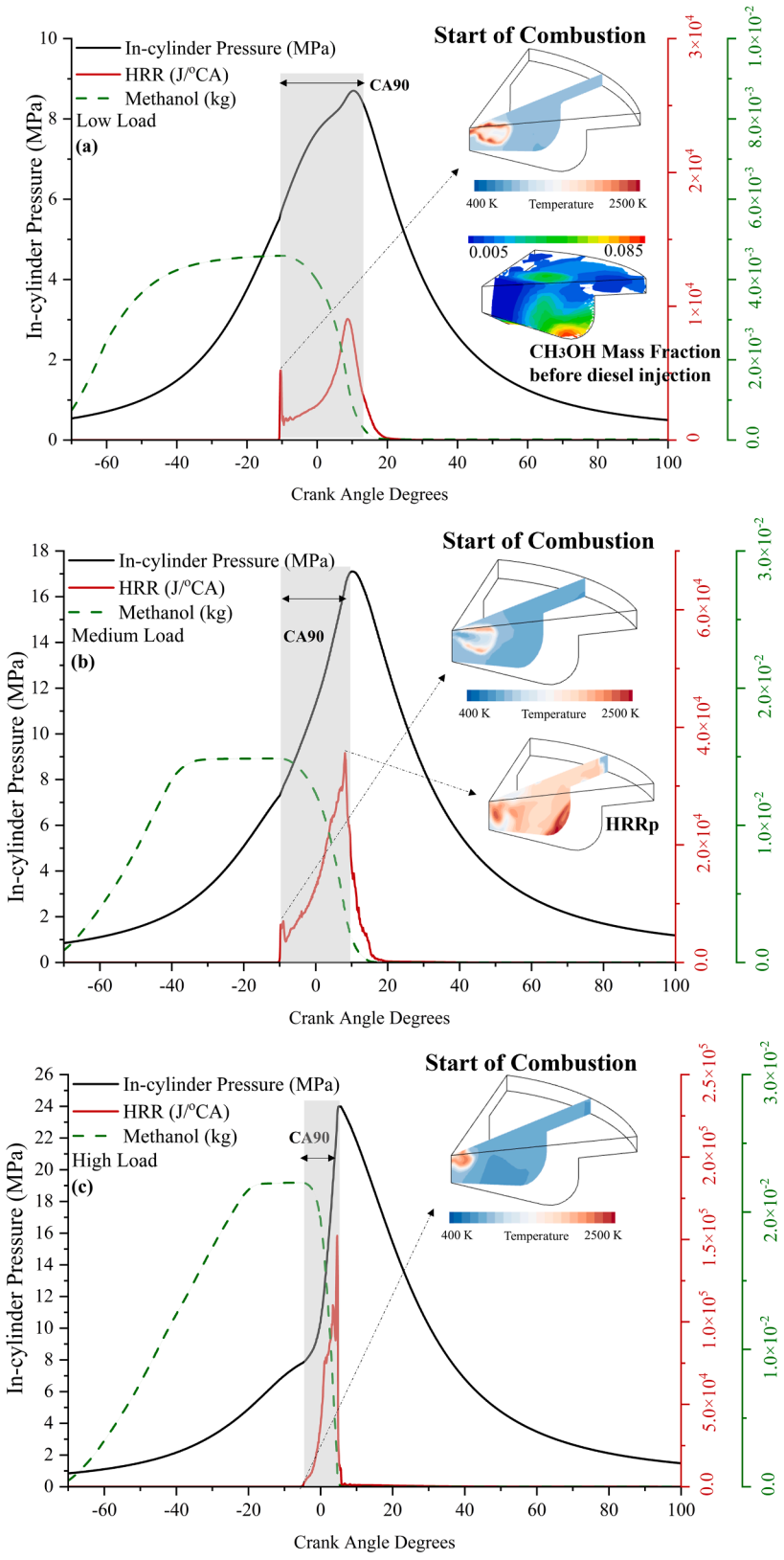

Fig. 9. In-cylinder pressure and heat release rate for the selected injection parameters at three different loads.

the emissions exceed the Tier III limit. However, the weight of this operating point is 20%, it does not impact the engine compliance. It is inferred that the investigated marine engine operation in the methanol–diesel (dual fuel) mode complies with the international NOx regulations without the need of after-treatment systems.

Fig. 11 presents the spatial distribution of in-cylinder temperature and NOx mass for the engine operation with the optimal settings in the low, medium, and high-load operation. For the lowload, the combustion starts at 9 °CA BTDC as indicated by the considerable temperature increase (exceeding 1800 K, which is the NOx formation cut-off

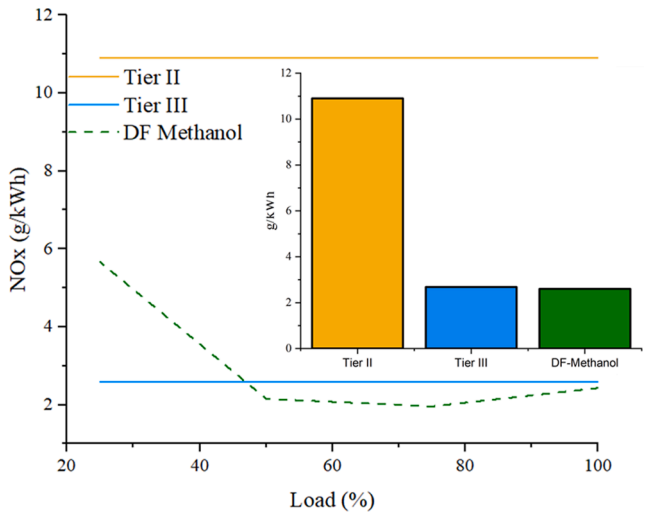

Fig. 10. NOx emissions IMO Tier II and III limits compliance.

temperature) of the flame front areas around the pilot diesel jet. The peak heat release rate is observed at 10 °CA ATDC, whereas the NOx formation is favoured around the injector area where local temperature exceed the cut-off value. Methanol combustion keeps occurring at 13 °CA ATDC, as indicated by the high temperature areas, with the NOx still being formed.

At medium-load operation (Fig. 11b), the combustion duration is reduced, and smaller ignition delay is observed. At 8 °CA ATDC the peak HRR is detected, and the diffusive flame front is observed at the bottom of the piston bowl. Therefore, NOx are created both close to the injector and piston bottom. Since the combustion duration is lowered, the residency time of the in-cylinder mixture in elevated temperature (< 1800 K) is reduced yielding smaller NOx concentration.

For the high load (Fig. 11c), the combustion duration significantly reduces compared to the other loads, whereas the temperature increase is more pronounced due to higher in-cylinder reactivity. Consequently, the NOx mass is greater compared to the medium load. The methanol combustion occurs rapidly in the areas close to the injector. The maximum heat release rate and NOx production are reached at 3 °CA ATDC. As 12% EGR is considered, the NOx emissions are lower compared to the low load.

4. Conclusions

This study performed a parametric optimisation of the injection timings for methanol and pilot diesel fuels in a methanol–diesel dual-fuel engine operating with 90 % methanol energy fraction. The aim was to determine the optimal injection settings for both fuels to minimise NOx emissions and enhance thermal efficiency across three engine load conditions. A computational fluid dynamics model was developed and validated to enable a detailed analysis of the in-cylinder combustion

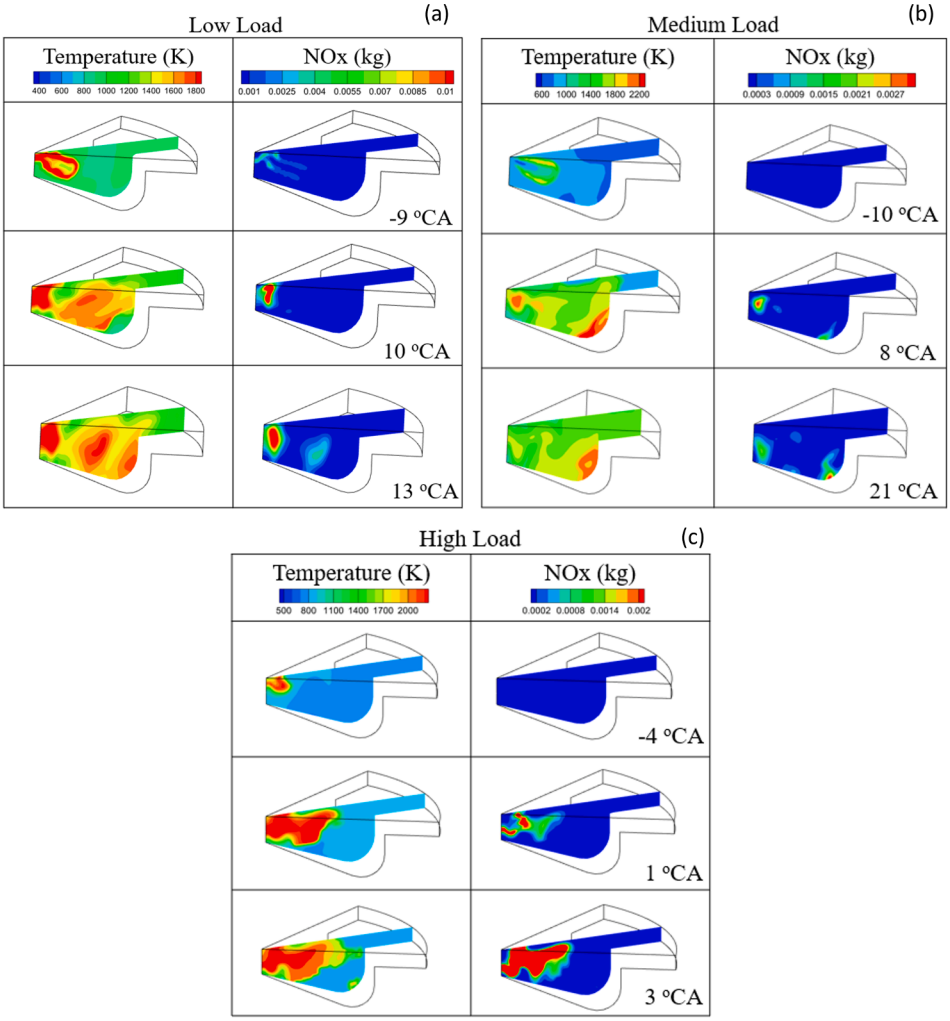

Fig. 11. Spatial analysis for temperature and NOx emissions at (a) low, (b) medium and (c) high load.

Table 7
Performance of the methanol engine under such conditions at different loads.

Load	Peak Firing Pressure	Peak HRR	Combustion Efficiency	Indicated Thermal Efficiency	NO_x emissions	UM emissions	CA50/CA90
	MPa	kJ	%	%	g/kWh	g/kWh	°CA ATDC
20 %	10.3	9.05	> 99 %	46	4.2	37.5	7/12.7
55 %	17.1	36.62		45	1.6	0.05	5.2/10.7
90 %	23.9	152.2		43	2.4	1.38	2.8/4.7

behaviour.

The results concluded that the optimal injection timings yielding minimal unburned methanol and NOx concentrations are 80°CA BTDC for methanol and 12 °CA BTDC for diesel, respectively. These settings facilitate sufficient air-methanol mixing and reduces peak temperatures, directly impacting NOx emissions and combustion efficiency. The proposed optimal methanol and diesel injection timing yielded NOx emissions of 4.2 g/kWh, 1.63 g/kWh and 5.29 g/kWh as well as indicated thermal efficiency of 48%, 45.3%, 43%, for the low, medium and high loads, respectively. The identified optimal injection settings render the investigated engine to comply with IMO Tier III NOx emission regulations without the need for additional NOx after-treatment.

It is evident that further knock mitigation techniques are required to broaden the injection timing envelope at high loads, allowing more cases to comply with the rate of pressure rise limits. It was deduced that that knock mitigation techniques are required to broaden the injection timing envelope at high loads, considering the required limit for the maximum rate of in-cylinder pressure rise limits. The derived results indicate that the engine settings optimisation can facilitate the simultaneous efficiency improvement and NOx emissions reduction whilst satisfying the unburnt methanol constraint, hence meeting operational requirements for marine engines. Hence, this study provides insights on the methanol fuelled marine engines challenges, contributing to the methanol uptake in shipping and its decarbonisation. The study is limited by the quantity of experimental data available to validate methanol combustion under operational conditions. Future studies should include engines of different sizes to assess the scalability of the findings. Furthermore, other alternative fuels options such as hydrogen and ammonia will be examined following the same optimisation method. Additionally, a multi-objective optimisation of the engine's geometrical characteristics is anticipated to positively influence the uptake of methanol fuel in maritime applications.

Declaration of competing interest

The authors declare that they have no known competing financial interests or personal relationships that could have appeared to influence the work reported in this paper.

Acknowledgments

The authors greatly acknowledge the funding from DNV AS and RCCL for the MSRC establishment and operation. The opinions expressed herein are those of the authors and should not be construed to reflect the views of DNV AS and RCCL. Authors would like to thank ARCHIE-WEST support for providing computational resources and CONVERGE CFD for the computational software license.

Appendix A

The discretising methodology follows the one provided in [43]. The governing equations for the modelled in-cylinder sector include the continuity, momentum, energy and species transport equations, which are presented as follows.

$$\frac{\partial \rho}{\partial t} + \nabla(\rho \vec{u}) = 0 \tag{A1}$$

Where,ρ, t and u denote the density, time and velocity vector, respectively.

$$\frac{\partial(\rho \vec{u})}{\partial t} + \nabla(\rho \vec{u}\vec{u}) = -\nabla p + \nabla(\tau) + \rho \vec{g} \tag{A2}$$

Where p denotes the pressure, $\vec{g}$ is the gravitational acceleration vector and τ is the viscous stress tensor.

$$\frac{\partial(\rho E)}{\partial t} + \nabla[\vec{u}(\rho E + p)] = \nabla(k_t \nabla T) + S \tag{A3}$$

Where E is the total energy per unit mass, k is the turbulent kinetic energy, T denotes the temperature, whereas S denotes the source term in (W/m^3).

$$\frac{\partial(\rho Y_i)}{\partial t} + \nabla(\rho Y_i \vec{u}) = \nabla(D \nabla Y_i) + R_i \tag{A4}$$

Where Y_i is the mass fraction of species i, D is the diffusion coefficient, and R_i represents the source term for species reaction.

The droplet breakup sub-model is represented by the Kelvin-Helmholtz and Rayleigh-Taylor instability models, which calculate the droplet breakup timescale (τ_{KH}) and wavelength (λ_{KH}) according to the following equations:

$$\tau_{KH} = B_o \frac{d}{\sqrt{\frac{\sigma}{\rho_l}}} \tag{A5}$$

$$\lambda_{KH} = C_0 d \left(\frac{\rho_g}{\rho_l}\right)^{\frac{1}{2}} \tag{A6}$$

Where d is the droplet diameter, σ is the Surface tension and ρ_l, ρ_g are the liquid and gas densities.

The turbulence model employed in the Reynolds averaged numerical simulation k-ε that governs turbulent flow with two transport equations:

$$\frac{\partial(\rho k_k)}{\partial t} + \frac{\partial(\rho k_k u_i)}{\partial x_i} = \frac{\partial}{\partial x_j}\left[\left(\mu + \frac{\mu_t}{\sigma_k}\right)\frac{\partial k_k}{\partial x_j}\right] + G_k - \rho\varepsilon$$

$$\frac{\partial(\rho\varepsilon)}{\partial t} + \frac{\partial(\rho\varepsilon u_i)}{\partial x_i} = \frac{\partial}{\partial x_j}\left[\left(\mu + \frac{\mu_t}{\sigma_\varepsilon}\right)\frac{\partial \varepsilon}{\partial x_j}\right] + \frac{C_{1\varepsilon}\varepsilon}{k}G_k - \frac{C_{2\varepsilon}\rho\varepsilon^2}{k}$$

Where k is the turbulent kinetic energy, μ is the turbulent viscosity, $C_{1,2}$ model constants, G_k turbulence production term, ε is the dissipation rate of turbulent kinetic energy.

Appendix B

The CFD model with natural gas operation, results for the in-cylinder maximum pressure and indicated power along with the respective experimentally measured values from the W50DF marine engine shop tests and percentage errors are presented in Table A1. The estimated percentage errors are below 4.1 % for the in-cylinder maximum pressure and 8.6 % for the indicating power, thus indicating adequately validated CFD model.

Further validation of the used methanol combustion mechanism for a light-duty diesel engine operating at 30 % methanol energy fraction with premixed methanol combustion in 75 % load was carried out. The derived CFD and measured in-cylinder pressure and HRR are presented in Fig. A1. These results denote that the developed CFD model is adequate for the case studies modelled herein.

Table A1
. Validation of the natural gas operation of the marine engine with shop trial data.

Load (%)	Indicated Power (kW)		Percentage Error (%)	Maximum cylinder Pressure (MPa)		Percentage Error (%)	NOx emissions (g/kWh)		Percentage Error (%)
	Measured	CFD		Measured	CFD		Measured	CFD	
25	1950	1900	3.6	3.8	3.8	0	9.15	9.9	8.6
50	3900	3950	2.3	6.4	6.6	4.1	9.7	10.1	4
75	5850	5700	3.6	9.2	9.0	3.2	9.7	10.4	7.8
100	7800	7890	2.2	12.6	12.5	1.8	9.43	10	6.7

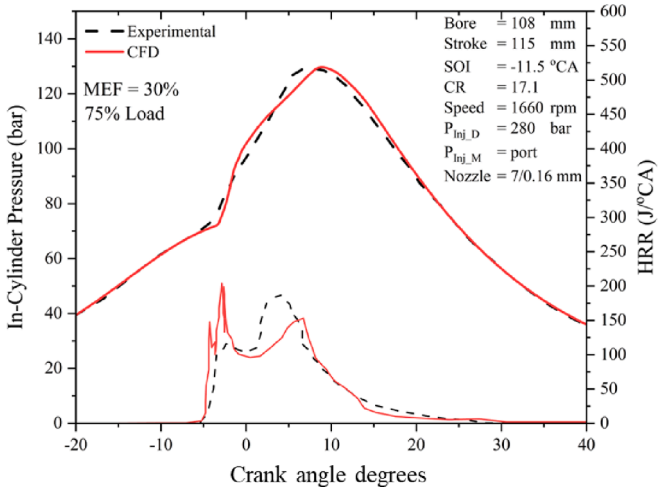

Fig. A1. Measurements and CFD results for the in-cylinder pressure and heat release rate for the for modelled light duty high-speed diesel engine [39].

Appendix C

To investigate if the identified start of injection timings are applicable to intermediate loads, two cases in 40 % and 70 % loads are modelled. The results presented in Fig. A2 demonstrate the almost complete methanol combustion and are in alignment with the results presented in the main text. At 40 % load combustion is slower and the heat release profile is characterised by a small, premixed part attributed to methanol-air mixing, and a diffusive part between 8 °CA BTDC and 18 °CA ATDC. The latter is the peak heat release point where the rate of burn of methanol is maximised. At 70 % load, combustion is shorter and the premixed part of the heat release rate drastically reduced. Peak heat release is achieved close to 8 °CA ATDC.

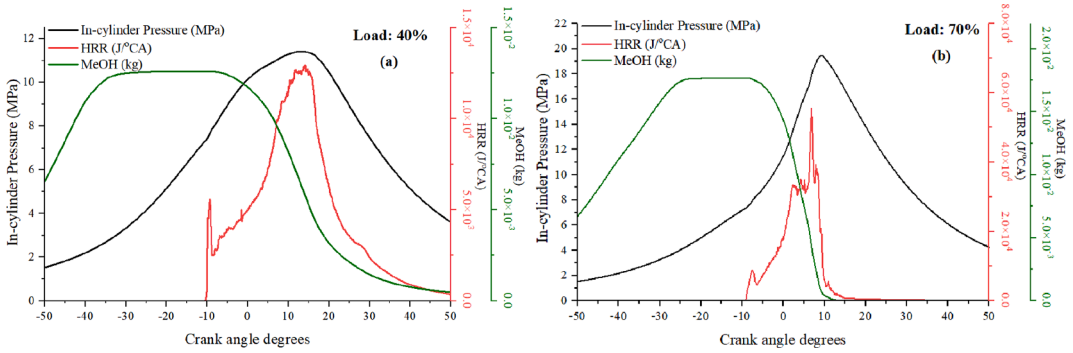

Fig. A2. In-cylinder pressure, heat release rate and unburnt methanol mass for (a) 40 % load and (b) 70 % load.

Data availability

No data was used for the research described in the article.

References

[1] M.A. Russo, J. Leitão, C. Gama, J. Ferreira, A. Monteiro, Shipping emissions over Europe: a state-of-the-art and comparative analysis, Atmos. Environ. 177 (2018) 187–194.

[2] P. Karvounis, C. Tsoumpris, E. Boulougouris, G. Theotokatos, Recent advances for sustainable and safe marine engines operation with alternative fuels, Front. Mech. Eng. 8 (2022).

[3] C.J. McKinlay, S.R. Turnock, D.A. Hudson, Route to zero emission shipping: Hydrogen, ammonia or methanol? Int. J. Hydrogen Energy 46 (55) (2021) 28282–28297.

[4] J. Shi, Y. Zhu, Y. Feng, J. Yang, C. Xia, A prompt decarbonization pathway for shipping: green hydrogen, ammonia, and methanol production and utilization in marine engines, Atmos. 14 (3) (2023) 584.

[5] P. Karvounis, G. Theotokatos, I. Vlaskos, A. Hatziapostolou, Methanol combustion characteristics in compression ignition engines: a critical review, Energies 16 (24) (2023) 8069.

[6] Z. Li, Y. Wang, H. Geng, X. Zhen, M. Liu, S. Xu, C. Li, Parametric study of a diesel engine fueled with directly injected methanol and pilot diesel, Fuel 256 (2019) 115882.

[7] S. Park, J. Cho, J. Park, S. Song, Numerical study of the performance and NOx emission of a diesel-methanol dual-fuel engine using multi-objective pareto optimization, Energy 124 (2017) 272–283.

[8] Q. Wang, C. Yao, Z. Dou, B. Wang, T. Wu, Effect of intake pre-heating and injection timing on combustion and emission characteristics of a methanol fumigated diesel engine at part load, Fuel 159 (2015) 796–802.

[9] M.R. Saxena, R.K. Maurya, Experimental investigation on range of fuel premixing ratio for stable engine operation of dual fuel engine using port injection of gasoline/methanol and direct injection of diesel, Adv. Energy Res. 2 (2020) 393–403.

[10] Rodriguez-Fernandez, J.; Hernandez, J.J.; Ramos, Á.; Barba, J.; Perez, V.M.D.; Torres, O.H.; Alonso, V.C.; Aragon, L.J.R. Optimization of the Operating Conditions of a Dual CI Engine Fueled with Methanol; SAE Technical Paper 2022-01-0465; SAE Mobilus: Washington, DC, USA, 2022.

[11] R. Sener, M.U. Yangaz, M.Z. Gul, Effects of injection strategy and combustion chamber modification on a single-cylinder diesel engine, Fuel 266 (2020) 117122.

[12] Enoki, K.; Hayashi, S.; Sawa, N. Optimum Injection Timings of Gas-Oil and Methanol in Dual Fuel CI Engine. In Proceedings of the 1993 International Off-Highway Powerplant Congress Exposition, Milwaukee, WI, USA, 13–15 September 1993.

[13] L. Ning, Q. Duan, H. Kou, K. Zeng, Parametric study on effects of methanol injection timing and methanol substitution percentage on combustion and emissions of methanol/diesel dual-fuel direct injection engine at full load, Fuel 279 (2020) 118424.

[14] Y. Li, M. Jia, L. Xu, X.S. Bai, Multiple-objective optimization of methanol/diesel dual-fuel engine at low loads: a comparison of reactivity controlled compression ignition (RCCI) and direct dual fuel stratification (DDFS) strategies, Fuel 262 (2019) 116673.

[15] Y. Li, Y. Cai, M. Jia, Y. Wang, X. Su, L. Li, A full-parameter computational optimization of both injection parameters and injector layouts for a methanol/diesel dual-fuel direct injection compression ignition engine, Fuel 1 (369) (2024) 131733.

[16] M. Shi, B. Wu, J. Wang, S. Jin, T. Chen, Optimization of methanol/diesel dual-fuel engines at low load condition for heavy-duty vehicles to operated at high substitution ratio by using single-hole injector for direct injection of methanol, Appl. Therm. Eng. 2 (2024) 122854.

[17] D.K. Soni, R. Gupta, Optimization of methanol powered diesel engine: A CFD approach, Appl. Therm. Eng. 5 (106) (2016) 390–398.

[18] P. Karvounis, G. Theotokatos, C. Patil, L. Xiang, Y. Ding, Parametric investigation of diesel–methanol dual fuel marine engines with port and direct injection, Fuel 381 (2025) 133441, https://doi.org/10.1016/j.fuel.2024.133441.

[19] K.M. Tsitsilonis, G. Theotokatos, C. Patil, A. Coraddu, Health assessment framework of marine engines enabled by digital twins, Int. J. Engine Res. 24 (7) (2023) 3264–3281.

[20] Heywood JB. Fluid motion within the cylinder of internal combustion engines—the 1986 Freeman scholar lecture.

[21] Y.B. Zeldovich, The oxidation of nitrogen in combustion explosions, Acta Physicochimica u.s.s.r. 21 (1946) 577–628.

[22] Z. Li, Y. Wang, H. Geng, X. Zhen, M. Liu, S. Xu, C. Li, Effects of diesel and methanol injection timing on combustion, performance, and emissions of a diesel engine fueled with directly injected methanol and pilot diesel, Appl. Therm. Eng. 25 (163) (2019) 114234.

[23] Wartsila 46 Project Guide available at https://brandhub.wartsila.com/m/39438d6bb2d10bd3/original/Wartsila-46F-Product-guide.pdf?utm_source=engines&utm_medium=dieselengines&utm_term=w46f&utm_content=productguide&utm_campaign=mp-engines-and-generating-sets-gated.

[24] C. Gong, L. Peng, Y. Chen, J. Liu, F. Liu, Y. Han, Computational study of intake temperature effects on mixture formation, combustion and unregulated emissions of a DISI methanol engine during cold start, Fuel 234 (2018) 1269–1277.

[25] Z. Li, Y. Wang, Z. Yin, H. Geng, R. Zhu, X. Zhen, Effect of injection strategy on a diesel/methanol dual-fuel direct-injection engine, Appl. Therm. Eng. 5 (189) (2021) 116691.

[26] A. Özden, A. Procacci, R.M. Galassi, F. Contino, A. Parente, Incremental sampling methods for multi-fidelity surrogate modeling: application on a furnace operating in MILD combustion conditions, Appl. Therm. Eng. 1 (246) (2024) 122902.

[27] Z. Li, Y. Wang, Z. Yin, Z. Gao, Y. Wang, X. Zhen, To achieve high methanol substitution ratio and clean combustion on a diesel/methanol dual fuel engine: a comparison of diesel methanol compound combustion (DMCC) and direct dual fuel stratification (DDFS) strategies, Fuel 304 (2021) 121466.

[28] L. Chen, W. Zhao, R. Zhang, H. Wei, P. Jiaying, Flame characteristics and abnormal combustion of ammonia-diesel dual-fuel engine with considering ammonia energy fractions, Appl. Therm. Eng. 15 (245) (2024) 122858.

[29] ISO 8178-9:2012(en) Reciprocating internal combustion engines — Exhaust emission measurement — Part 9: Test cycles and test procedures for test bed measurement of exhaust gas smoke emissions from compression ignition engines operating under transient conditions.

[30] G. Huang, Z. Li, W. Zhao, Y. Zhang, J. Li, Z. He, Y. Qian, L. Zhu, X. Lu, Effects of fuel injection strategies on combustion and emissions of intelligent charge compression ignition (ICCI) mode fueled with methanol and biodiesel, Fuel 15 (274) (2020) 117851.

[31] K.M. Tsitsilonis, G. Theotokatos, C. Patil, A. Coraddu, Health assessment framework of marine engines enabled by digital twins, Int. J. Engine Res. 12 (2023) 14680874221146835.

[32] J.C. Andrae, R.A. Head, HCCI experiments with gasoline surrogate fuels modeled by a semidetailed chemical kinetic model, Combust. Flame 156 (4) (2009) 842–851.

[33] M. Shi, B. Wu, J. Wang, S. Jin, T. Chen, Optimization of methanol/diesel dual-fuel engines at low load condition for heavy-duty vehicles to operated at high substitution ratio by using single-hole injector for direct injection of methanol, Appl. Therm. Eng. 1 (246) (2024) 122854.

[34] W. Yu, W. Yang, F. Zhao, Investigation of internal nozzle flow, spray and combustion characteristics fueled with diesel, gasoline and wide distillation fuel (WDF) based on a piezoelectric injector and a direct injection compression ignition engine, Appl. Therm. Eng. 5 (114) (2017) 905–920.

[35] N. Nordin, Complex chemistry modeling of diesel spray combustion, Chalmers University, 2001. PhD thesis.

[36] Z.Y. Han, R.D. Reitz, A temperature wall function formulation for variable density turbulence flows with application to engines convective heat transfer modeling, Int. J. Heat Mass Transf. 40 (3) (1997) 613–625.

[37] Z.Y. Han, Z. Xu, N. Trigui, Spray/wall interaction models for multidimensional engine simulation, Int. J. Eng. Res. 1 (1) (2000) 127–146.
[38] R. Payri, F.J. Salvador, J. De La Morena, V. Pagano, Using a one-dimensional spray model to improve liquid length and ignition delay estimations for diesel flames, Appl. Therm. Eng. 1 (124) (2017) 1090–1102.
[39] R. Zang, C. Yao, Numerical study of combustion and emission characteristics of a diesel/methanol dual fuel (DMDF) engine, Energy Fuel 29 (6) (2015) 3963–3971.
[40] M. Acaroglu, E. Baser, H. Aydogan, E. Canli, A new energy crop onopordum spp.: a research on biofuel properties, Energy 15 (261) (2022 Dec) 125305.
[41] A.H. Abdulkarim, A. Ates, K. Altinisik, E. Canli, Internal flow analysis of a porous burner via CFD, Int. J. Numer. Meth. Heat Fluid Flow 29 (8) (2019) 2666–2683.
[42] M.M. Ahmed, I.M. Eldesoky, A.G. Nasr, R.M. Abumandour, S.I. Abdelsalam, The profound effect of heat transfer on magnetic peristaltic flow of a couple stress fluid in an inclined annular tube, Mod. Phys. Lett. B 28 (2024) 2450233.
[43] M. Darbandi, M.S. Abdollahpour, M. Hasanpour-Matkolaei, A new developed semi-full-scale approach to facilitate the CFD simulation of shell and tube heat exchangers, Chem. Eng. Sci. 14 (245) (2021) 116836.
[44] X. Liang, Z. Zheng, H. Zhang, Y. Wang, H. Yu, A review of early injection strategy in premixed combustion engines, Applied Sciences. 9 (18) (2019 Sep 7) 3737.